Understanding the effects of copolymerized cellulose nanofibers and diatomite nanocomposite on blend chitosan films

Muhammad Mujtaba [a,b,c,*], Rut Fernández-Marín [c], Eduardo Robles [c,d], Jalel Labidi [c], Bahar Akyuz Yilmaz [e], Houwaida Nefzi [f]

[a] *Department of Bioproducts and Biosystems, School of Chemical Engineering, Aalto University, FI-00076 Aalto, Finland*
[b] *Institute of Biotechnology, Ankara University, Ankara 06110, Turkey*
[c] *Biorefinery Processes Research Group, Department of Chemical and Environmental Engineering, University of the Basque Country UPV/EHU, Plaza Europa 1, 20018 Donostia-San Sebastián, Spain*
[d] *University of Pau and the Adour Region, E2S UPPA, CNRS, Institute of Analytical and Physicochemical Sciences for the Environment and Materials (IPREM-UMR 5254), 371 Rue du Ruisseau, 40004 Mont de Marsan, France*
[e] *Department of Biotechnology and Molecular Biology, Faculty of Science and Letters, Aksaray University, 68100 Aksaray, Turkey*
[f] *Laboratory of Materials, Molecules and Applications, IPEST, Preparatory Institute of Scientific and Technical Studies of Tunis, Tunisia*

ARTICLE INFO

ABSTRACT

Chitosan films lack various important physicochemical properties and need to be supplemented with reinforcing agents to bridge the gap. Herein, we have produced chitosan composite films supplemented with copolymerized (with polyacrylonitrile monomers) cellulose nanofibers and diatomite nanocomposite at different concentrations. The incorporation of CNFs and diatomite enhanced the physicochemical properties of the films. The mechanical characteristics and hydrophobicity of the films were observed to be improved after incorporating the copolymerized CNFs/diatomite composite at different concentrations (CNFs: 1%, 2% and 5%; diatomite: 10% and 30%). The antioxidant activity gradually increased with an increasing concentration (1–5% and 10–30%) of copolymerized CNFs/diatomite composite in the chitosan matrix. Moreover, the water solubility decreased from 30% for chitosan control film (CH-0) to 21.06% for films containing 30% diatomite and 5% CNFs (CNFs-D30-5). The scanning electron micrographs showed an overall uniform distribution of copolymerized CNFs/diatomite composite in the chitosan matrix with punctual agglomerations.

1. Introduction

Besides the numerous desirable features offered by carbohydrate polymers (especially chitosan), still a huge potential of improvement is present in its physicochemical (hydrophilicity, low mechanical properties, weak barrier characteristics) and biological properties (antioxidants, enhanced antimicrobial activity) for competing in the industry (Mujtaba, Morsi, et al., 2019). For this purpose, researchers focus on blending many ingredients such as nanocrystals or nanoparticles of other polysaccharides and essential oils to enhance the physical and biological properties of these biopolymer-based films up to an acceptable level.

Chitosan is a deacetylated derivative of chitin, one of the largest available biomass found on the face of the planet after cellulose. The major sources of chitin include marine wastes such as crabs, shrimps,

and other crustaceans. Besides, chitin can be also be extracted from various species of insects and fungi (Sharif et al., 2018). Thanks to its desirable characteristics such as biodegradability, non-toxicity, biocompatibility, and antimicrobial activity, chitosan exhibits several applications in different industrial areas such as food coating, cosmetics, medicine, agriculture, and biomedical (Wang et al., 2018). Being cationic polymer chitosan inhibits the growth of microorganisms such as bacteria and fungi (Kong et al., 2010). The excellent film-forming ability of chitosan makes it an ideal ingredient for coating and packaging applications. Numerous studies have reported the production of chitosan film for food packaging and fruit coating (Fan et al., 2009; Rambabu et al., 2019; Tripathi et al., 2009; Wu et al., 2018). However, the practical use of chitosan-based films for packaging is restricted due to poor mechanical and barrier properties. The improvement in these properties can be accomplished by making composite films with other reinforcing

---

ingredients such as cellulose nanocrystals/nanofibers (Mujtaba et al., 2017), chitin nanocrystals (Wu et al., 2019), starch (Duan et al., 2011), gelatin (Pereda et al., 2011), and diatomite (Tamburaci & Tihminlioglu, 2017), etc. In a study by Wu et al. (2018) quaternized chitosan films were produced by incorporating laponite immobilized silver nanoparticles and tested for litchis conservation. In another report, a composite film was produced by incorporating nano-cellulose into chitosan, gelatin, and starch matrices. A gradual increase in nano-cellulose content results in the improvement of mechanical and food conservation properties of the composite films (Noorbakhsh-Soltani et al., 2018). These nanofillers offer numerous advantages over synthetic ones i.e., low production cost, large quantities of raw source, and sustainability (Mujtaba, Morsi, et al., 2019).

Cellulose fibers have been used as a reinforcing material in different matrices, thanks to their excellent mechanical properties, low production cost, renewability, large surface area, high aspect ratio, outstanding flexibility, and low thermal expansion (Mujtaba et al., 2018). Cellulose is a largely founded biomass on the face of the earth, and its sources include cotton, microorganisms, plant leaves, grasses, and waste papers (Pennells et al., 2020). The incorporation of cellulose nanofibers even at low concentration could impart higher stiffness, thanks to its high aspect ratio Besides, cellulose nano fibers (CNFs) also make interconnected networks with a matrix of other materials through hydrogen bonding (Zhang et al., 2020). As it is known that chitosan-based films suffer from low thermal, mechanical, and barrier properties. The above-mentioned characteristics of CNFs make it an ideal reinforcing ingredient for polymer composite like chitosan. For this purpose, CNFs (from different sources and in different forms) have been blended with chitosan to produce novel composites with enhanced physicochemical properties that can broaden the application areas of chitosan-based composite (H. P.S. et al., 2016). Xu et al. (2019), produced chitosan films reinforced with CNFs and reported 2.3 times increase in tensile strength, improved water vapor permeability, transparency and solubility of the composite films. Edible packaging films were produced by adding CNFs at different concentrations into chitosan matrix (with different molecular weight) resulted in enhanced barriers and antibacterial properties (Deng et al., 2017).

Diatomaceous earth is a natural siliceous rock, which has been found as the accumulated protective skeletons of diatoms. Diatoms have a unique ability to absorb silica from seawater to produce their skeleton (Tamburaci & Tihminlioglu, 2017). More than 85% of the diatomaceous beds are comprised up of metal oxides with SiO_2 backfill. Diatoms are non-motile, single-celled eukaryotic microalgae (Akyuz et al., 2017). The surface of silica has silanol groups, which serve as active sites for bonding with other compounds. As is known from the literature, the water-soluble fraction of diatom is less than 1%, making it an ideal ingredient for enhancing the hydrophobicity of biopolymer-based edible films (Xu et al., 2005). Diatom has been used as a reinforcing material for the chitosan matrix in many studies. Akyuz et al. (2017), incorporated diatomaceous earth into chitosan film at different concentrations. The authors have reported important enhancement in different physicochemical properties of composite films, such as; enhanced wettability (77° to 92°), improved mechanical (elongation at break; 3% to 3.5%) and thermal properties (Tg; 184 °C to 204 °C). Besides, diatomite has been composited to chitosan film for different applications including; hydrogel for triboelectric generator and self-powered tremor sensor (Kim et al., 2021), skin-attachable chitosan-diatom triboelectric nanogenerator (Kim et al., 2020), chitosan/dopamine/diatom-biosilica composite beads for rapid blood coagulation (Liang et al., 2018). Considering all these studies so far, the combined effect of CNFs and diatomite on the overall physicochemical properties of chitosan composite films have not been reported. Given this, we assume that the incorporation of *co*-polymerized cellulose/diatomite nanocomposite will enhance the physicochemical (mechanical, hydrophobicity) and biological (antioxidant) properties of chitosan blend films.

Graft copolymerization is an efficient route to obtain polymers with modified surfaces that can serve different purposes (Gürdağ & Sarmad, 2013). This kind of biodegradable copolymer graft can be produced through a ceric ion-mediated redox polymerization reaction. Ceric ions are flexible reagents that oxidize the functional groups of organic materials via the radical pathway. In the process of grafting, copolymerization occurred because of the bonding of the side chains to the main polymer (cellulose) resulting in a branched structure. Copolymers comprised of natural materials are thought to be more prone to biodegradation than synthetic polymers (Maiti et al., 2013). The cellulose-based graft copolymer is developed to modify certain physicochemical properties of CNFs. Hydrophobic monomers such as styrene, acrylonitrile and vinyl acetate, etc. are used to improve the compatibility and adhesion of hydrophilic CNFs to the hydrophobic components of other materials (Roy et al., 2005). Similarly, in the current study, a graft copolymer of CNFs was produced by using acrylonitrile, as a monomer to enhance its adhesion and compatibility with diatomite.

So far, to the best of our knowledge, no study has reported the combined effect of copolymerized CNFs/diatomite composite on the physical, chemical, and biological properties of chitosan-based nanocomposite films. This is why herein; we incorporated copolymerized CNFs and CNFs/diatomite nanocomposite into the chitosan matrix. The produced nanocomposite films were studied for their physicochemical and biological characteristics using the available analytical tools and assays.

2. Materials and methods

2.1. Materials

Chitosan powder (Mw 500.000 g/mol and degree of deacetylation of 98%) was kindly supplied by Mahtani Chitosan Pvt. Ltd., India. Glacial acetic acid (96%, technical grade) was purchased from Panreac AppliChem. Cellulose nanofibers (CNFs) (average length; 607 ± 85 nm and average width; 68 ± 22 nm, surface charge; −24 mV) were extracted as reported in previous work (Robles et al., 2018). Raw diatomaceous earth (DE) was purchased from Gafsa, Tunisia. Hydrochloric acid (HCl), 37%, was purchased from Panreac. Acrylonitrile monomer, ceric ammonium nitrate (CAN), acetone (≥99.9%, 58.08 g/mol), and nitric acid (65%, 1.39 kg/L) were purchased from Sigma Aldrich, USA and were used as received. Type II water was used during all steps of the experiment.

2.2. Diatomite purification

The raw DE was crushed and dissolved in 2 M HCl with continuous stirring (350 rpm) for 1 h at room temperature (25 °C). The obtained material was then filter washed using a 0.45-μm membrane with distilled water several times until the pH becomes neutral. The purified diatomite was dried inside an oven at 100 °C for 24 h. The sample was stored in closed containers for further use.

2.3. Synthesis of cellulose nanofibers-graft-polyacrylonitrile

Cellulose nanofibers-graft-polyacrylonitrile (CNF-Ac) was obtained by following a method reported by Kalaoğlu et al. (2016) with minor modifications. Briefly, 3 g (3% dry weight) of CNFs were dispersed in 100 ml water and stirred at 35 °C for 15 min using a magnetic stirrer. For the polymerization reaction, a 3 M acrylonitrile (80 ml) and 13.46 mM cerium ammonium nitrate were added dropwise (2 drops sec^{-1}) to the cellulose suspension for 10 min. Cerium ammonium nitrate solution was prepared in a 100 ml 0.1 M nitric acid solution. The reaction was stopped after 1 h by pouring the mixture into 500 ml cold water. The obtained copolymerized (modified) CNFs were first filtered-washed (0.45 μm membrane) with acetone to remove impurities and distilled water until the pH became neutral. The final copolymerized product was dried at 50 °C for 24 h.

2.4. Synthesis of copolymerized-CNF/diatom nanocomposites

The nanocomposite of nitrilated cellulose and diatomite (CNF-D) was obtained using the same conditions as in Section 2.3 with two different concentrations of diatomite, being 10% (w/w) and 30% (w/w). In brief, CNF-Ac were suspended in Type II water, followed by diatomite to the mass of the final copolymer. The mixture was stirred at 35 °C for 24 h using a magnetic stirrer. The obtained samples were filtered, washed, and oven-dried at 50 °C.

2.5. Chitosan composite film preparation

Chitosan-based nanocomposite films with CNFs, CNF-Ac, and CNF-D were prepared by incorporating them into a 1% chitosan solution (1 g chitosan dissolved in 1% acetic acid solution at room temperature using a magnetic stirrer) at three different concentrations, being 1%, 2%, and 5%. 20% glycerol to the total weight of chitosan was added to all the solutions as a plasticizer. The mixture was stirred using a Heidolph Silent Crusher M at 12,000 rpm for 15 min to ensure well-dispersed film solution. Film solutions were subjected sonicaiton (100 W and 10 mins) using an ultrasonic cell crusher (Scientz-IID, Xinzhi Biotech Co., Ltd., Ningbo, China). Sonication was conducted to further ensure, the preparation homogenous solution and to prevent any possible aggregation of diatomite and CNFs in the matrix. The film solutions were homogenized and poured into Petri dishes and kept at 30 °C for 48 h. for drying. After drying, the films were peeled off and stored in the same ventilated climatic chamber at 25 ± 1 °C and 30 ± 1% relative humidity before the measurements (Kurek et al., 2012; Schreiber et al., 2013). Besides, a blank sample called CH-0 was produced. Table 1 summarizes the different samples and their composition; moreover, the films' final aspect can be appreciated in Fig. 1.

2.6. Physicochemical analysis

2.6.1. Chemical properties

The diatomite sample (before and after the treatment) was analyzed by the XRF technique using a PANalytical AXIOS (WDXRF) spectrometer to determine its chemical composition.

FT-IR spectra of the films were measured using a PerkinElmer Spectrum Two FT-IR spectrometer with built-in universal attenuated total reflectance fitment having a diamond crystal lens with internal reflection. Spectra were measured in the range of 600 and 4000 cm^{-1}
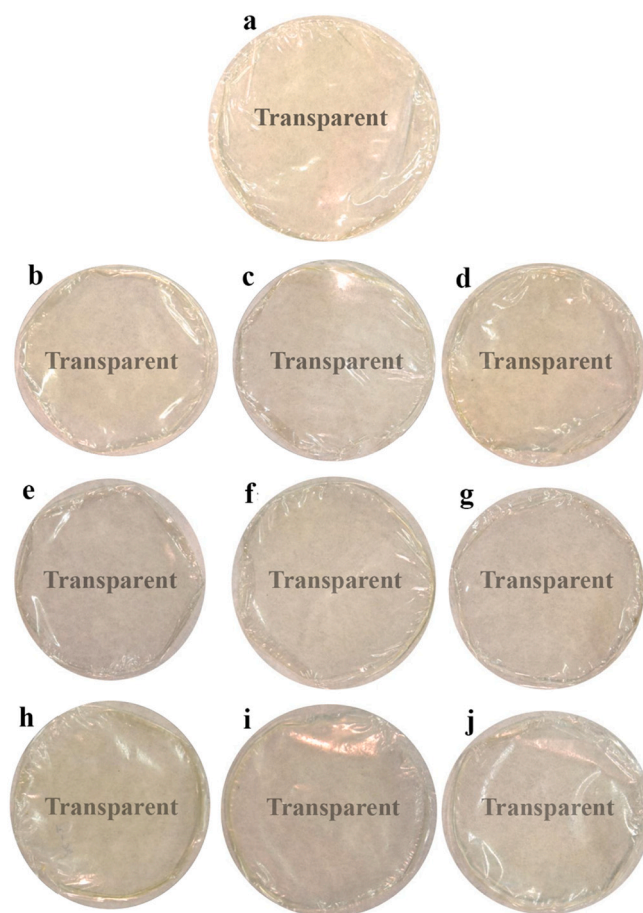

Fig. 1. Visual aspect: a) CH-0, b) CNF-1, c) CNF-2, d) CNF-5, e) CNF-D10-1, f) CNF-D10-2, g) CNF-D10-5, h) CNF-D30-1, i) CNF-D30-2, j) CNF-D30-5.

with a resolution of 8 cm^{-1}.

DPPH (2.2′-diphenyl-1-picrylhydrazyl) radical scavenging activity of the produced composite films was analyzed following the methodology described in our previous study (Kaya et al., 2018). Besides, for reader convenience, detailed methods are also provided in supporting information.

2.6.2. Thermal properties

TGA-DTG analysis was carried out to investigate the thermal strength of the composite film samples. The analysis was conducted following the standard procedure (ASTM E1131-08) (Earnest, 1988) with a TGA/SDTA 851 Mettler Toledo instrument with a ≈5 mg film sample taken and used for each analysis. The heating was applied at a continuous rate of 10 °C min^{-1} from 25 to 600 °C under a nitrogen atmosphere of 20 ml min^{-1}.

The endothermic and exothermic characteristics of the film samples were investigated via DSC analysis. For this purpose, Mettler Toledo DSC822e (Schwerzenbach, Switzerland) was used with an N$_2$ atmosphere and a temperature range between 50 and 400 °C. Around 50 mg of film sample was taken for each film. Film samples were positioned in hermetic aluminum pans with a heating scan set at 5 °C min^{-1}.

2.6.3. Physical properties

The mechanical properties were analyzed with a Material Testing Systems (MTS Insight 10) device using a load cell of 250 N and a deformation rate of 5 mm min^{-1}. The analysis was performed under ambient conditions (temperature; 25 ± 1 °C and relative humidity; 50 ± 5%) (ASTM, 1995). For analysis, the samples were cut into strips measuring 5 mm in width and 40 mm in length. Mechanical properties

Table 1
Sample codes used throughout the manuscript and the thickness of the prepared films.

Sample	Chitosan (%)	CNF (%)	CNF-polyacrylonitrile (%)	Diatomite (%)	Thickness (μm)
CH	100	–	–	–	52
CNF-1	99	1	–	–	60
CNF-2	98	2	–	–	62
CNF-5	95	5	–	–	70
CNF-Ac-1	99	–	1	–	71
CNF-Ac-2	98	–	2	–	86
CNF-Ac-5	95	–	5	–	89
CNF-D10–1	89	–	1	10	88
CNF-D10–2	88	–	2	10	89
CNF-D10–5	85	–	5	10	89
CNF-D30–1	69	–	1	30	94
CNF-D30–2	68	–	2	30	99
CNF-D30–5	65	–	5	30	105

were calculated using MTS Test Works 4 software. The results presented are an average of eight determinations.

The morphology of all the film samples was carried out by scanning electron microscopy (Hitachi Ltd., Japan). The samples were coated with 20 nm of gold under a high vacuum. The scanning was measured using 10 kV acceleration voltage and $1000\times$ as a magnification value.

The contact angle measurements were taken by an OCA20 (Data-Physics Instruments GmbH, Germany) video-based contact angle measurement system. Accurate sessile drop volume was measured through a software-controlled dosing volume weight drop. The contact angle was measured by using water. For each film sample were taken eight measurements.

2.6.4. Optical properties

The opacity of the film samples was measured with a UV–Vis spectrophotometer V-630 (JASCO, Japan) according to Fernández-Marín et al. (2020) method with some modification by the following equation:

$$Opacity = \frac{Abs_{600}}{x} \quad (1)$$

Abs600 is the value of absorbance at 600 nm, and x represents the thickness (mm). Three replications were determined for each film.

The light transmittance (%) of the film samples was determined by using a UV–Vis spectrophotometer V-630 with a wavelength range between 250 and 750 nm. Samples were measured in triplicate in small rectangles with size 10×45 mm^2.

Color properties of the different composites were measured with the CIELab color space to study the influence of the selected copolymers in the visual aspect of chitosan films. The color was measured with a PCE-CMS 7 (PCE Instruments, Spain) colorimeter over ten different regions of each composite. The films were placed on a standard white plate (L*: 93.4, a*: −0.3133, b*:0.3194) and the parameters L* (lightness), a* (red-green), and b*(yellow–blue) were measured at five different locations of the film surface and the average value was calculated. Color changes were calculated as the difference between composites and the blank (chitosan film) was calculated with the equation:

$$\Delta E = \sqrt{(\Delta a^*)^2 + (\Delta b^*)^2 + (\Delta L^*)^2} \quad (2)$$

$$Wi = 100 - \sqrt{(100 - L)^2 + a^2 + b^2} \quad (3)$$

$$\Delta E = \sqrt{(\Delta a^*)^2 + (\Delta b^*)^2 + (\Delta L^*)^2} \quad (4)$$

$$C_{ab}^* = 180 + arctg\left(\frac{b}{a}\right) : a < 0 \quad (5)$$

$$h_{ab}^* = 180 + arctg\left(\frac{b}{a}\right) : a < 0 \quad (6)$$

ΔE^* represents the color change, and L* represents the lightness, and a* and b* represent chromate coordinates from which color combination can be determined.

2.6.5. Soil degradation and water solubility

The soil degradation and water solubility of the produced composite films were analyzed following the protocols with minor modifications described in our previous research (Mujtaba, Koc, et al., 2019). A detailed methodology is provided in supporting information.

2.7. Statistical analysis

Statistical Analysis Software (version 8; SAS Institute, 2005, Cary, NC, USA) was used to conduct the data analysis. The TABULATE procedure was used to calculate descriptive statistics while ANOVA. The means were separated using Tukey's test at 5% significant level when they were significant.

3. Results

3.1. Thickness

The thickness of the produced composite films has revealed notable differences. For CH-0, thickness was recorded as 52 μm. The incorporation of CNFs and diatomite earth enhanced the overall thickness up to a 105 μm in CNF-D30-5. The incorporation of diatomite and CNF gradually increased the thickness of composite films i.e., CNF-D30-1, CNF-D30-2 and CNF-D30-5. Current results were found in line with previous reports (Mujtaba, Koc, et al., 2019).

3.2. Chemical properties

The chemical quantification and purity of diatomite are presented in Table S1. The SiO$_2$ present in the DE was 29.60%, with minor amounts of other minerals residues. After acid hydrolysis in 2 M HCl, the SiO$_2$ of diatomite increased to 79.74%; this agrees with other reports where the SiO$_2$ content of diatomite from different sources was found between 62.80 and 90.10% (H. Nefzi et al., 2018).

FT-IR was used for investigating the structural interactions between chitosan, diatomite, and CNF revealed by possible shifts in bands. Fig. 2 presents the spectra of diatomaceous earth (DE) and purified diatomite (PD) as well as the different nanocomposite films. In the spectra of DE and PD, the two absorption bands in the spectrum of DE at 3350 cm^{-1} and 1650 cm^{-1} correspond to the O—H vibration of the structural hydroxyl groups. The bands at 1023 cm^{-1} and 671 cm^{-1} are attributed to the asymmetric stretching vibration mode of siloxane (Si-O-Si). Besides, the band at 786 cm^{-1} corresponds to Al-O-Si stretching vibration in DE. The two bands at 876 and 1431 cm^{-1} can be attributed to the calcite impurities. However, after the acid hydrolysis, these bands have disappeared, confirming the elimination of impurities in DE (Nefzi et al., 2018).

The infrared spectrum of CH-0 presents a broad absorption between 3000 and 3400 cm^{-1}, due to the overlapping of the hydroxyl group and amino group stretching vibration (Labidi et al., 2016). The two small bands at 2900 cm^{-1} and 2850 cm^{-1} are attributed to the -CH$_2$-stretching. The absorption band at 1650 cm^{-1} belongs to amide I, while the two bands at 1535 and 1550 cm^{-1} represent the N—H (amide II band) of chitosan carbon chains. The bands at 1261, 1160, and 1023 cm^{-1} are attributed to the NH-CO group, the C-O-C, and the C=O stretch, respectively (Ahyat et al., 2017).

Different specific bands confirm the interaction between CNF-D composite with chitosan. Cellulose nanofibers and chitosan share a large set of similar functional groups such as hydroxyl (OH) stretching vibration, alkane C—H stretching vibration, and C—O stretching vibration. The bands at 3000 and 3400 cm^{-1} can be assigned as OH bands attributed to the hydroxyl and amino groups stretching vibration (Romainor et al., 2014). On the other hand, the successful copolymerization with polyacrylonitrile was confirmed by the presence of an absorption band at 2200 cm^{-1} assigned to the CN triple bond (Anitha et al., 2015). Bands at 2850 and 1550 cm^{-1} can be attributed to alkane C—H stretching vibration for cellulose and chitosan. Furthermore, the band at 1715 cm^{-1} corresponds to C=O (Nefzi et al., 2019). The incorporation of CNFs and diatomite at different concentrations to chitosan film leads to changes in the intensity of determined bands. Chitosan, diatomite, and CNF exhibit almost similar peaks for specific functional groups. The adsorption band at the range 3000 and 3400 cm^{-1} is related to the O—H vibration of the physically absorbed H$_2$O; the structural hydroxyl groups and amino group stretching vibration bands were also recorded. The absorption band at 1650 cm^{-1} belongs to amide I. The two bands at 1535 and 1550 cm^{-1} represent the N—H (amide II band) of chitosan carbon chains. Major changes have been recorded in the intensities of the band at 1716 cm^{-1}, which corresponds to the carboxyl groups
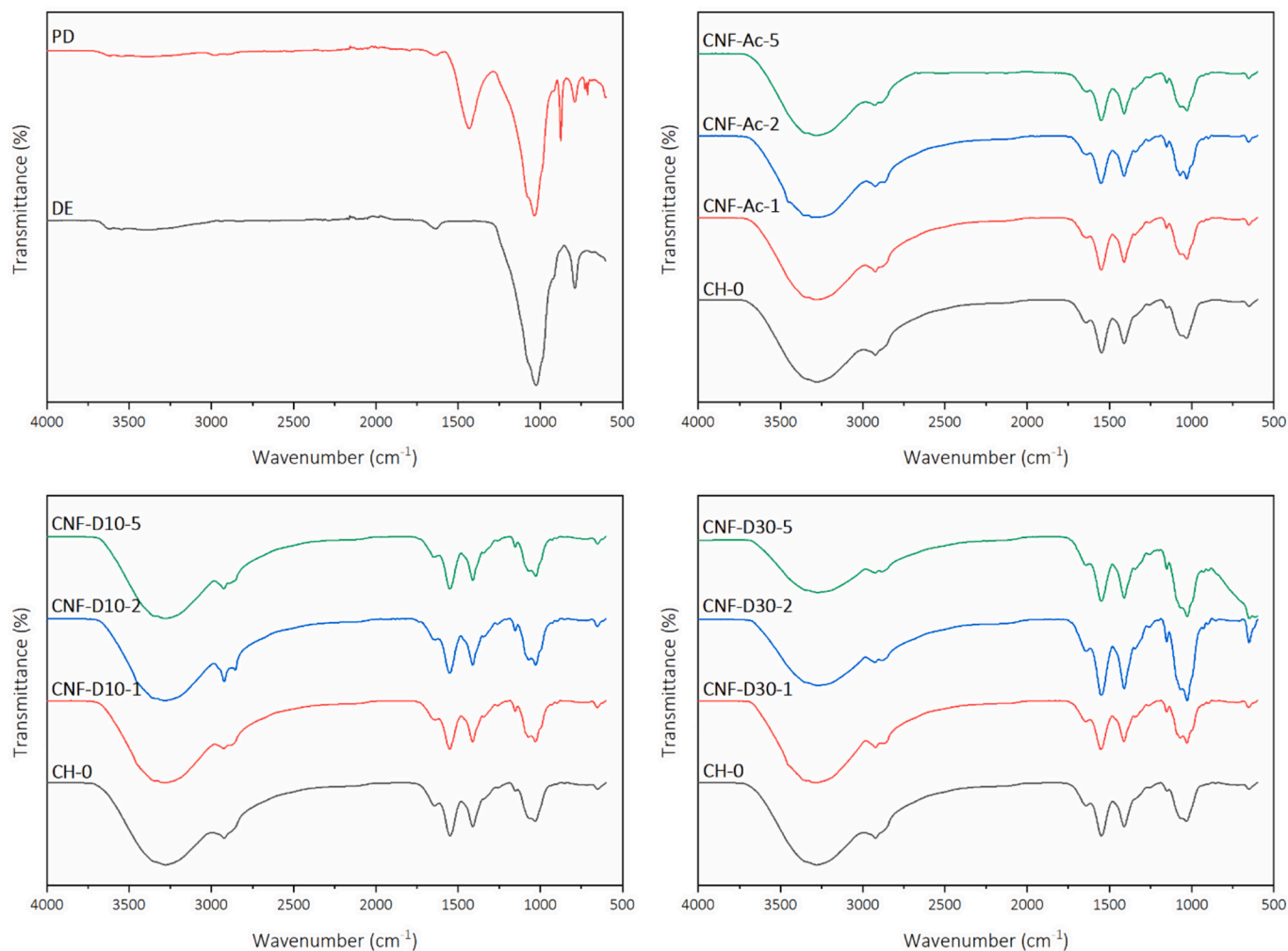
Fig. 2. FT-IR spectra of copolymerized cellulose nanofibers and copolymerized cellulose nanofibers/diatomite/chitosan composite films (DE: diatomaceous earth, PD: purified diatomite).

(C=O). The two small bands at 2900 cm^{-1} and 2850 cm^{-1} are due to the -CH$_2$- stretching. Two vibrations can identify the high amount of SiO$_2$ groups in diatomite at 1023 cm^{-1} and 671 cm^{-1}, which are related to the asymmetric stretching vibration mode of siloxane (Si-O-Si). The bands at 1261 cm^{-1} and 1160 cm^{-1} are attributed to the NH-CO and C-O-C groups.

DPPH assays were performed for the composite film samples to investigate their antioxidant properties. DPPH radical scavenging activity of CH-0 film was 17.84%. The incorporation of CNFs contributed to the overall antioxidant activity of the composite films. For CNF-1, CNF-2, and CNF-5, the records were 21.41%, 24.70%, and 27.34%, respectively. The antioxidant activity increased slightly, compared to the control; similarly, a previous study showed that DPPH antioxidant activity decreased with the increase of CNF in chitosan composite films (Resende et al., 2018). Though the chitosan and CNF exhibit low antioxidant activities, but blending these polysaccharides together, an increase in the antioxidant activities of the composite films was recorded. Furthermore, as it is known that chitosan and cellulose are both polysaccharides, and upon their combination, the reducing ends of the materials may open, thus enhancing the antioxidant activities of the films. The antioxidant activity is the interaction of free radicals with the hydroxyl groups, and free amino groups of the chitosan and cellulose (Hai et al., 2020). For CNF-Ac-1, CNF-Ac-2, and CNF-Ac-5 films, the DPPH activity was 26.18%, 21.30%, and 25.09%, respectively, showing that the copolymerization of CNF with polyacrylonitrile increased the

antioxidant activity of composite films. For CNF-D10-1, CNF-D10-2, and CNF-D10-5, the DPPH activity was recorded as 24.5%. 21.80% and 24.05%, respectively; while for CNF-D30-1, CNF-D30-2, and CNF-D30-5 it was 24.70%, 28.14%, and 30.27%, respectively. However, no significant variation was recorded among the films reinforced with CNF and diatomite. In a study by Akyuz et al. (2017), the authors reported a non-significant contribution of diatomite towards the antioxidant activity of chitosan-based composite films.

3.3. Thermal properties

The thermal behaviors of the composite films were examined through thermal gravimetric analysis, and the results obtained are shown in Fig. 3; Table S2 presents the thermal degradation peaks and the residue at 600 °C. DTG curves were characterized by three different decomposition steps corresponding to the maximum degradation rate at T_{max}. The first mass loss was recorded at ≈70–76 °C for all the film samples. This first mass loss can be attributed to the evaporation of physically adsorbed or mechanically compacted water (Tirkistani, 1998). The second mass loss in CH-0 was observed at 188.2 °C, and it can be ascribed to the degradation of glycerol, as the thermal degradation temperature of glycerol is in the range of 170–220 °C (Cardenas & Miranda, 2004). The third mass loss observed in CH-0 at 273.43 °C is linked to chitosan degradation (Khan et al., 2012). This peak was observed close to 275 °C in reinforced films. The thermal degradation
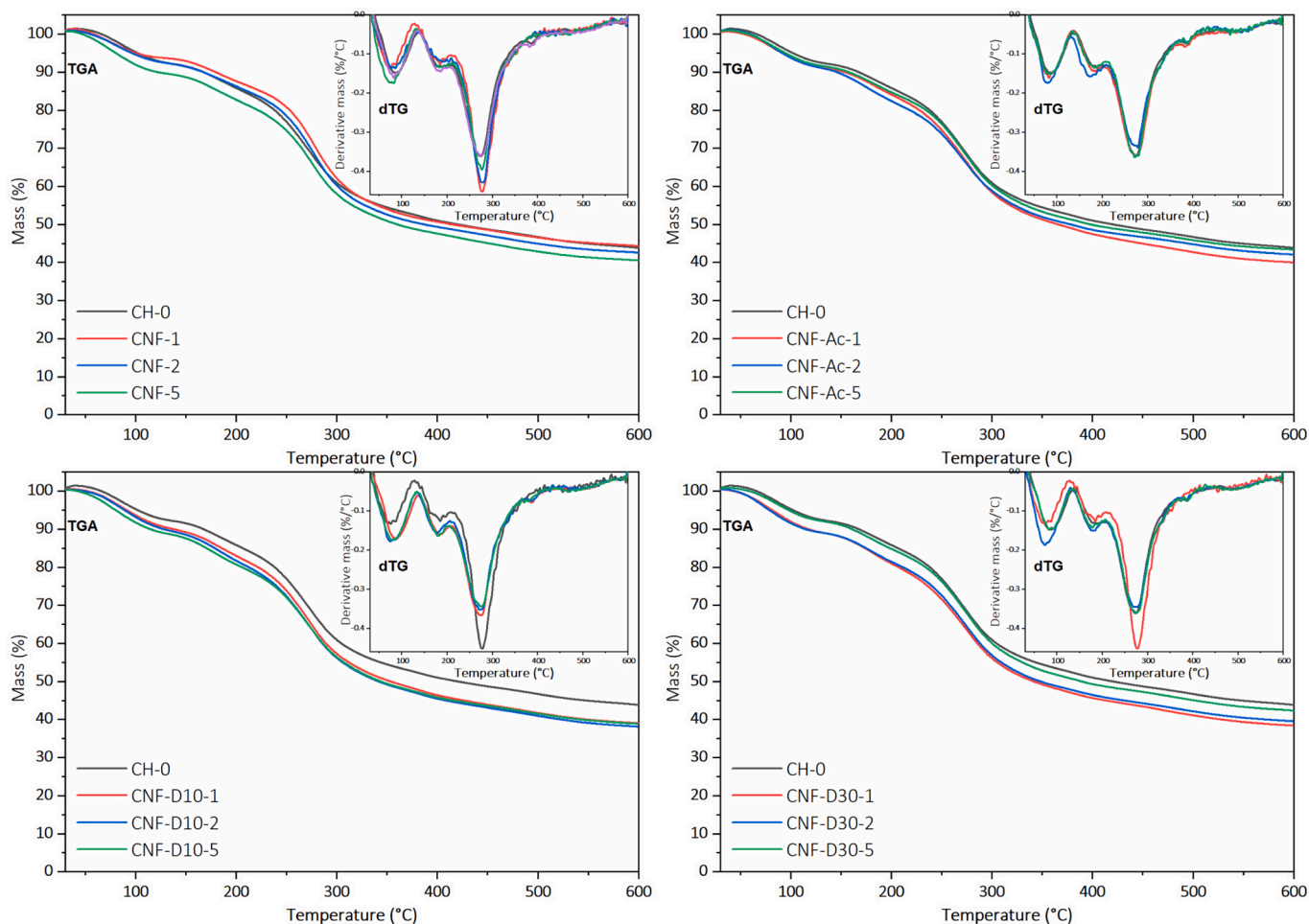
Fig. 3. TGA-dTG thermograms of copolymerized cellulose nanofibers and copolymerized cellulose nanofibers/diatomite/chitosan composite films.

temperature for CNF is known to be around 330 °C (Xu et al., 2015). However, in the current study, no significant changes were observed in the thermal stability of composite films as the decomposition temperatures of CH-0 and films with CNF were similar. This can be due to the crosslinking of polyacrylonitrile added to the structure. The principal mass loss for all the composite films at 270–280 °C was ≈40%.

On the other hand, films with CNF had higher residue at first but diminished with the increase of cellulose share (CNF-1 44.2%, CNF-2 42.5%, and CNF-5 40.5%). In the case of copolymerized CNF, residues increased in proportion with the increase of CNF-Ac from 39.9% in CNF-Ac-1 to 43.3% in CNF-Ac-5. In CNF-D films, CNF-D10-1, CNF-D10-2, and CNF-D10-5 presented similar residues; however, CNF-D30-1, CNF-D30-2, and CNF-D30-5 showed an increase in residue proportionally related to the content of CNF-D. Considering the literature reports, nearly similar changes were in the thermal behavior of chitosan-based films incorporated with CNFs were reported. The incorporation of cellulose nanocrystals into the chitosan matrix (1%, 2% and 5%) resulted in degradation temperature around 277 °C. Similarly, Akyuz et al. (2017) reported the degradation of chitosan films incorporated with diatomite around 264–277 °C. These results support the TGA results in the current study.

Fig. 4 shows the DSC thermograms of the composite films. The detailed glass transition temperature (T_g) and enthalpies (ΔH) for the samples are given in Table S3. Three prominent peaks were observed; two endothermic and one exothermic. The first endothermic peak was in the range of 80 to 94 °C ($\Delta H \approx 78$–131 J g^{-1}) and is related to the evaporation of free and bound water from the structure of polysaccharides (Andonegi et al., 2020). The second endothermic peak

corresponded to the T_g. Although the T_g of chitosan largely depends on its molecular weight, degree of deacetylation, source, or extraction method, it is usually determined in the range of 150–200 °C (Dong et al., 2004; Sakurai et al., 2000). In the current study, the T_g of CH-0 was 184.5 °C and ΔH of 30.5 J g^{-1}. These results were observed to be in line with previous literature reports by Akyuz et al. (2017) in which Tg was 178.75 °C and ΔH of 21.98 J g^{-1}. The data demonstrated that the incorporation of CNF and diatomite has slightly increased the T_g values (Celebi & Kurt, 2015). The exothermic peaks appeared between 260 and 275 °C and were associated with the crystallization temperature of the chitosan with diatomite films (Akyuz et al., 2017). The film samples containing diatomite (CNF-D10 and CNF-D30) have revealed an increase in crystallization temperature (T_c) and enthalpy with increased diatomite content, being T_c: 262.9 °C and ΔH: 125.3 J g^{-1} for CNF-D10-5 and Tc: 264.2 °C and ΔH: 154.9 J g^{-1} for CNF-D30-5. This effect is produced by electrostatic interactions between chitosan and diatomite (Akyuz et al., 2017). In the CNF-Ac samples, the maximum temperature was around 280 °C and assigned to polyacrylonitrile cycling. Maximum temperature values decreased as the concentration of cellulose nanofibers increased (283.3 °C for CNF-Ac-1, 272.6 for CNF-Ac-2, and 261.4 °C for CNF-Ac-5). Therefore, the addition of chitosan and cellulose nanofibers could influence the polyacrylonitrile cycling mechanism (Kim & Lee, 2014). These results were observed to be in line with previous literature reports. Zhao et al. (2020) reported a notable shift of endothermic peaks to higher values after incorporating cellulose nanofibers in chitosan matrices. This increase was attributed to the abundance of hydrophilic groups which improve the water-polymer interaction. Similarly Akyuz et al. (2017) reported a slight increase
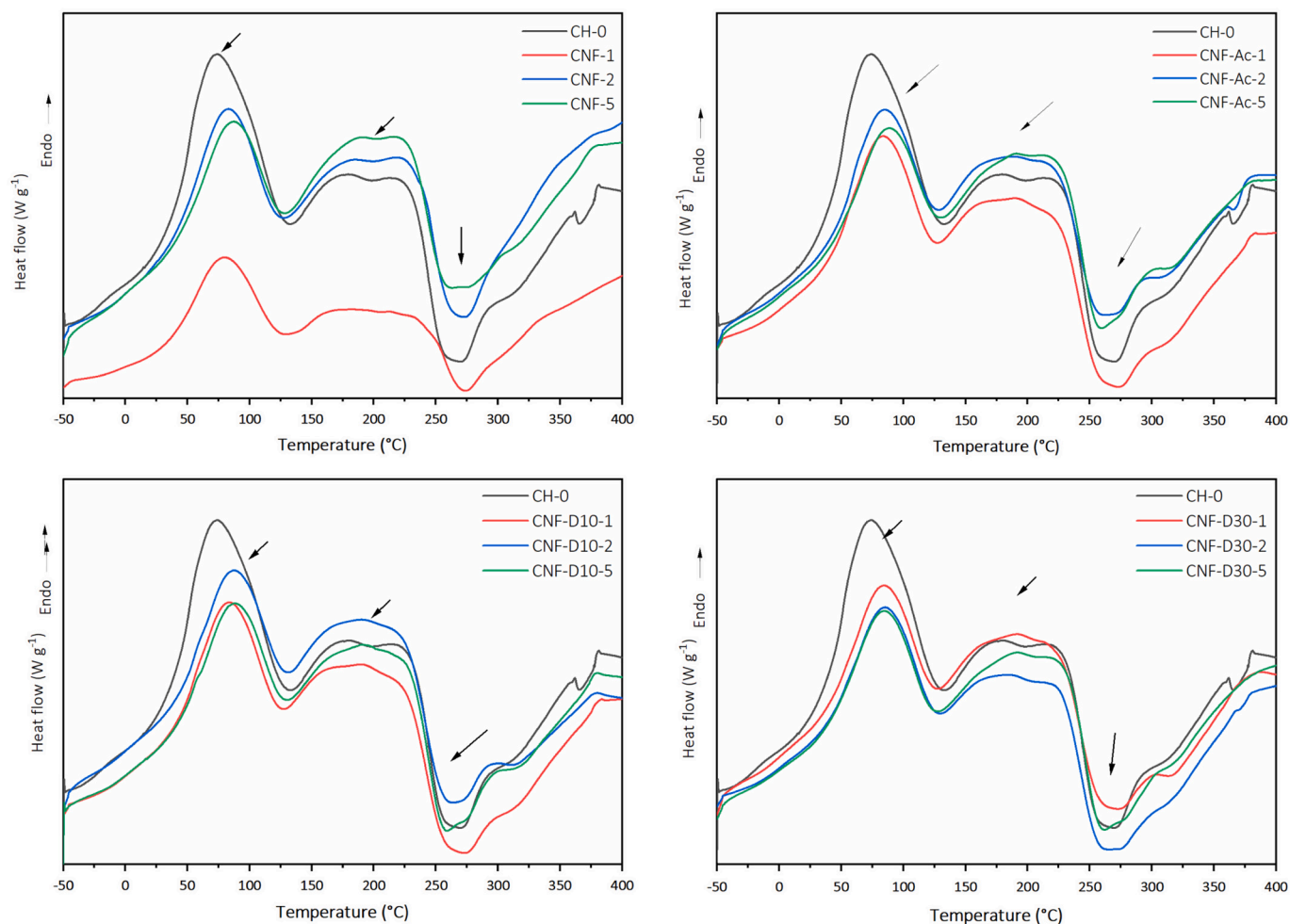
Fig. 4. Differential scanning calorimetry of the copolymerized cellulose nanofibers and copolymerized CNFs/diatomite/chitosan composite films.

(178 °C to 179 °C) in the overall thermal stability of chitosan based films incorporated with diatomite earth.

3.4. Physical properties

The mechanical properties of the composite films are presented in Fig. 5. The addition of CNF-Ac increases the strain of the films and makes them, in general, more resistant (tensile strength). In contrast, the addition of diatomite to the formulation resulted in a reduction of the strain of the films compared with CNF-Ac. At low share, they were also less flexible than chitosan. The explanation for such behavior comes from the nature of diatomite as being siliceous earth, which may store more energy, but will not contribute to the strain of a film. It is also observable when comparing CNF-D10 and CNF-D30, as strain at break is reduced between ≈43% and ≈68% to ≈41% and ≈57%. Another observable phenomenon occurring when adding CNF-Ac or CNF-D is an increase in the strain at mass content of 5%; this results in CNF-Ac-5 having a mean strain of ≈77%, CNF-D10 of ≈68%, and CNF-D30 of ≈57%. However, the standard error associated with those samples was considerably higher than that of films with lower reinforcement content. The cause for such instability might be related to an uneven distribution of the load inside the films, which allows having samples with agglomerations provoking interstitial breaks of the continuous film structure, thus increasing the possibility of fracture.

Regarding the ultimate tensile strength (UTS), it is appreciated a convex function, with a constant diminishing of the UTS at 2% content regarding 1%, which is then increased at 5% content; this replicates through all samples with no constable relation with the addition of diatomite, as the variations are relatively low. This implies that the central aspect influencing the UTS is the CNF-Ac, with 2% content having a higher presence of CNF-Ac and CNF-D than 1% through the continuous matrices, which gives their presence a negative implication in terms of strength. In contrast, the increase of CNF-Ac and CNF-D content results in a better distribution of the load, thus increasing the tensile strength. However, as for the strain, the higher content of CNF-Ac and CNF-D resulted in a less consistent behavior towards tensile stress.

Moduli presented a trend to increase with the presence of co-polymers, as well as diatomite charges. They were low in general, thus showing the high viscoelastic properties of the elaborated films. The addition of CNF increased the energy storage of the films, which was further increased when CNF-D was added as copolymers. However, as the amount of CNF-D increased (from 10 to 30), it can be seen that the error bars also tend to increase, as the presence of interstitial defects introduced by a low interaction between diatomite and chitosan causes higher variation between the samples, which suggests a less homogeneous material when the amount of inorganic charge is increased.

Contact angles were recorded to investigate the influence of the different CNF on the composite films; results are shown in Table S4. For CH-0, the contact angle was 87.3%. For chitosan films with CNF, the contact angle was between 78.8 ± 1.8 to 84.5 ± 1.61 degrees. Results revealed that the incorporation of cellulose nanofibers resulted in a slight decline in hydrophobicity. This decline can be due to the increase in hydrophilic groups (coming from CNF) in the matrix. This enhances the water-polymer interaction and consequently decrease the overall
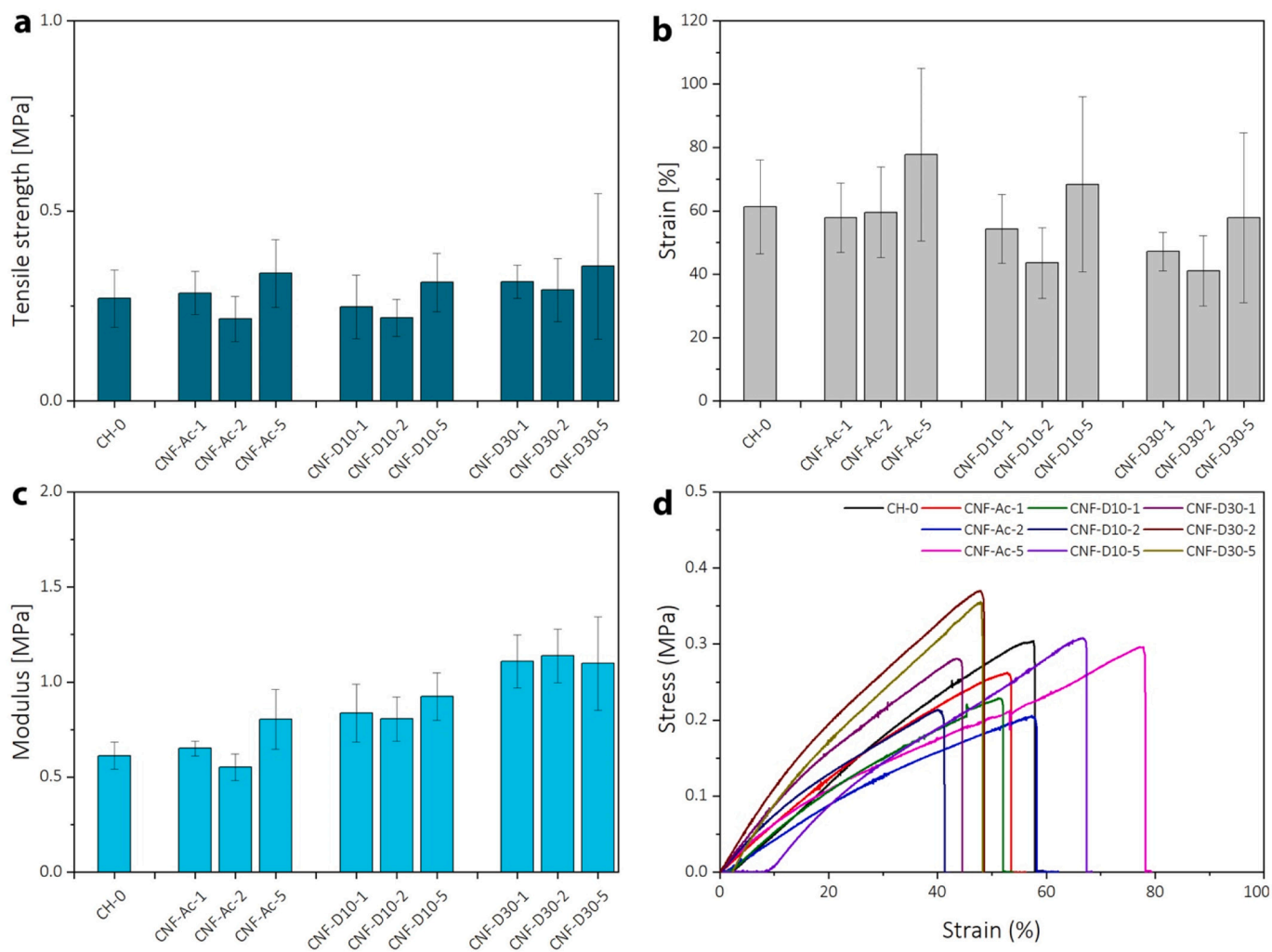
Fig. 5. Mechanical properties of copolymerized cellulose nanofibers and copolymerized cellulose nanofibers s/diatomite/chitosan composite films; a) tensile strength, b) strain, c) modulus, and d) stress/strain curves.

contact angle.

On the other hand, when the diatomite was incorporated into the composite films, the contact angle reached the hydrophobic range (90° ≤ θ ≤ 150°). For CNF-D10, the contact angle increases from 82.6 ± 0.78° to 95.3 ± 0.77°. While for CNF-D30, the contact angle was observed in the range of 94.7 ± 0.18° to 100 ± 0.91°. The incorporation of diatomite resulted in a significant increase in hydrophobicity of composite films. This increase in the contact angle can be ascribed to the extreme hydrophobic nature of diatomite. The solubility of diatomite is reported to be 1% of the total dry mass. The hydrophobic character of diatomite comes from the stable tetrahedral SiO_2 groups, making 85% of diatomite dry mass. The O atoms of SiO_2 interact with the amino group of chitosan through H bond, reducing the active sites for water molecules to interact (Akyuz et al., 2017). Thus, it resulted in an overall decrease in the hydrophilicity of chitosan composite films when increasing the diatomite concentration.

SEM was used to understand better the morphology of the nanocomposite film surfaces (Fig. 6). In the sample of pure chitosan (CH-0), a homogeneous and smooth surface was observed, giving the appearance of an ordered matrix (Jahed et al., 2017). In contrast, as the diatomite and cellulose nanofibers were added in the other samples, a more rugged and striated appearance was observed. However, the formation of grooves in some areas of the less crystalline films was also appreciated. The addition of diatomite particles showed a rough and irregular surface and the formation of blister-shaped structures due to the diatomite

(Fig. 8h–m). Besides, in the samples with the highest concentration of diatomite, the partial homogeneous distribution between cellulose nanofibers and diatomite particles was observed.

3.5. Optical properties

The opacity of the films is an important property to determine the film transparency for applications such as food packaging (Fernández-Marín et al., 2020). In the current study, the opacity values of the composite are in Fig. 7. The results revealed higher transparency with increased opacity values for the composite films. The lowest opacity value as 1.114 ± 0.126 was recorded for CH-0, which is similar to the literature (1.635 ± 0.003) (Priyadarshi et al., 2018). Moreover, the results showed that the film samples with the lowest concentration of CNF (CNF-1, CNF-2, CNF-Ac-1, CNF-Ac-2, CNF-D10-1, CNF-D10-2, CNF-D30-1, and CNF-D30-2) revealed lower opacity values as 1.5-4, which are considered as transparent (opacity <5) (Bonilla et al., 2018). However, the film samples with high concentrations of CNF (CNF-Ac-5, CNF-D10-5, and CNF-D30-5) resulted in higher opacity values >5. The incorporation of CNF increases the opacity of the films, which is also evident from the slightly yellow color of the films. These observations were found in accordance with a previous study reporting the cassava starch/chitosan/Gallic acid films reinforced with a 5% concentration of cellulose nanofibers (Zhao et al., 2019). The film samples reinforced with diatomite and cellulose nanofibers (CNF-D10-1, CNF-D10-2, CNF-D10-
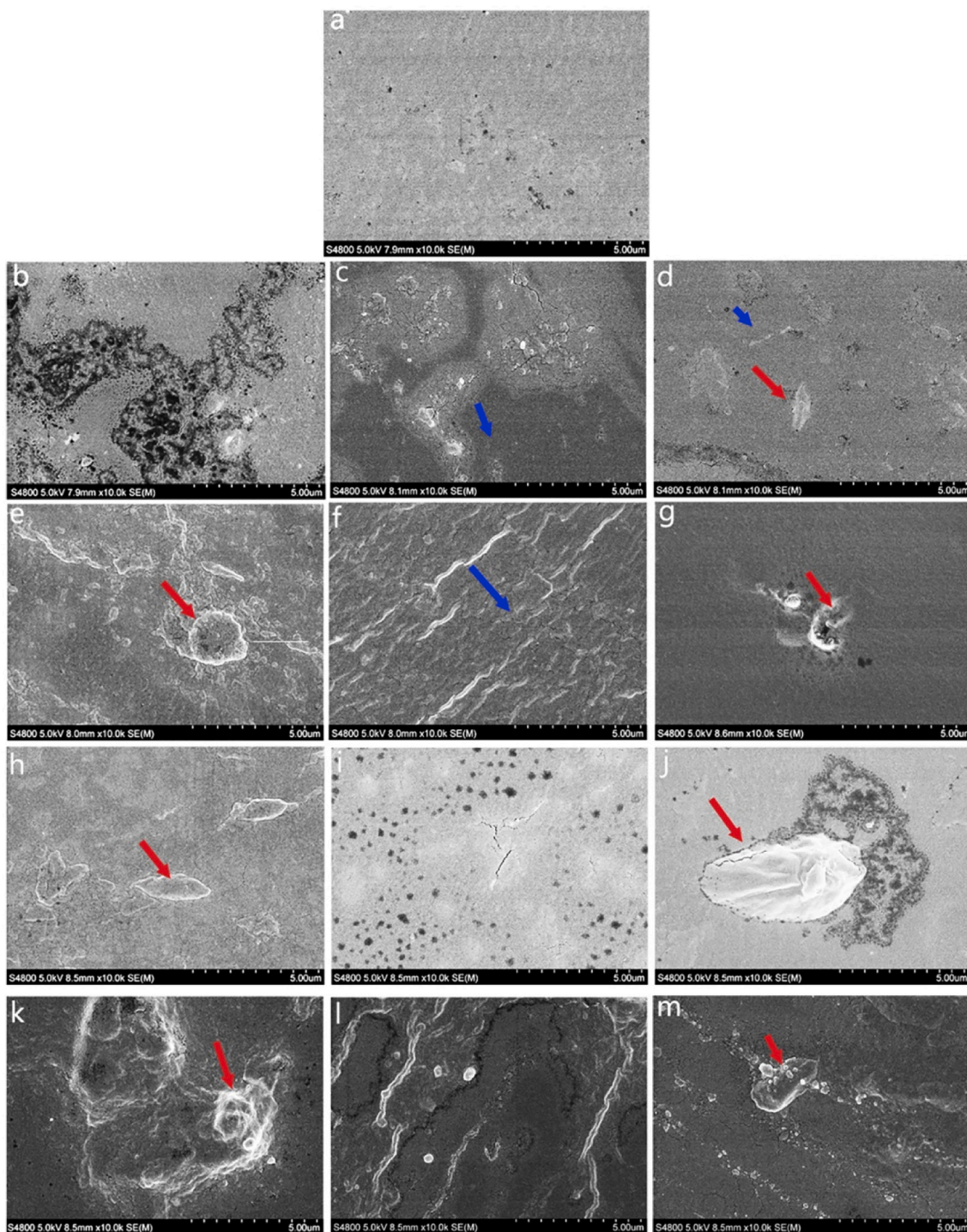
Fig. 6. SEM images of the surface of a) CH-0, b) CNF-1, c) CNF-2, d) CNF-5, e) CNF-Ac-1, f) CNF-Ac-2, g) CNF-Ac-5, h) CNF-D10-1, i) CNF-D10-2, j) CNF-D10-5, k) CNF-D30-1, l) CNF-D30-2, m) CNF-D30-5 (blue arrows; segregated fibers in composite films, red arrows; blister shaped structures).

5, CNF-D30-1, CNF-D30-2, and CNF-D30-5) revealed no significant variation in their opacity values even at increased concentrations of diatomite. In general, the opacity of the films increases with the rising of the cellulose nanofibers concentration.

Transparency is recognized as a crucial factor in food packaging, directly influencing consumer decisions about a product in both positive and negative ways (Soni et al., 2016). The protective barrier against UV–Vis light of the composite films was measured in the spectral range 245 to 750 nm. Fig. 8 presents the light transmittance curves. For CH-0, the maximum light transmittance (*Tr*) was recorded as 90%. Which is

similar to previous works Soni et al. (2016). The incorporation of CNF results in a decrease in the overall transmittance (*Tr*). Composite films with the highest percentage of CNF (CNF-5. CNF-Ac-5. CNF-D10-5 and CNF-D30-5) exhibited the lowest light transmission values being around 60% at 750 nm. Similar results were observed compared with literature, with 10% of cellulose whiskers in chitosan films Li et al. (2009). Increasing the CNF to 30% resulted in an increased *Tr* of 62%. Furthermore, the addition of diatomite (CNF-D10 and CNF-D30) decreased *Tr* % when compared to samples containing only CNF (CNF-1. CNF-2 and CNF-5). These results were observed similar to those
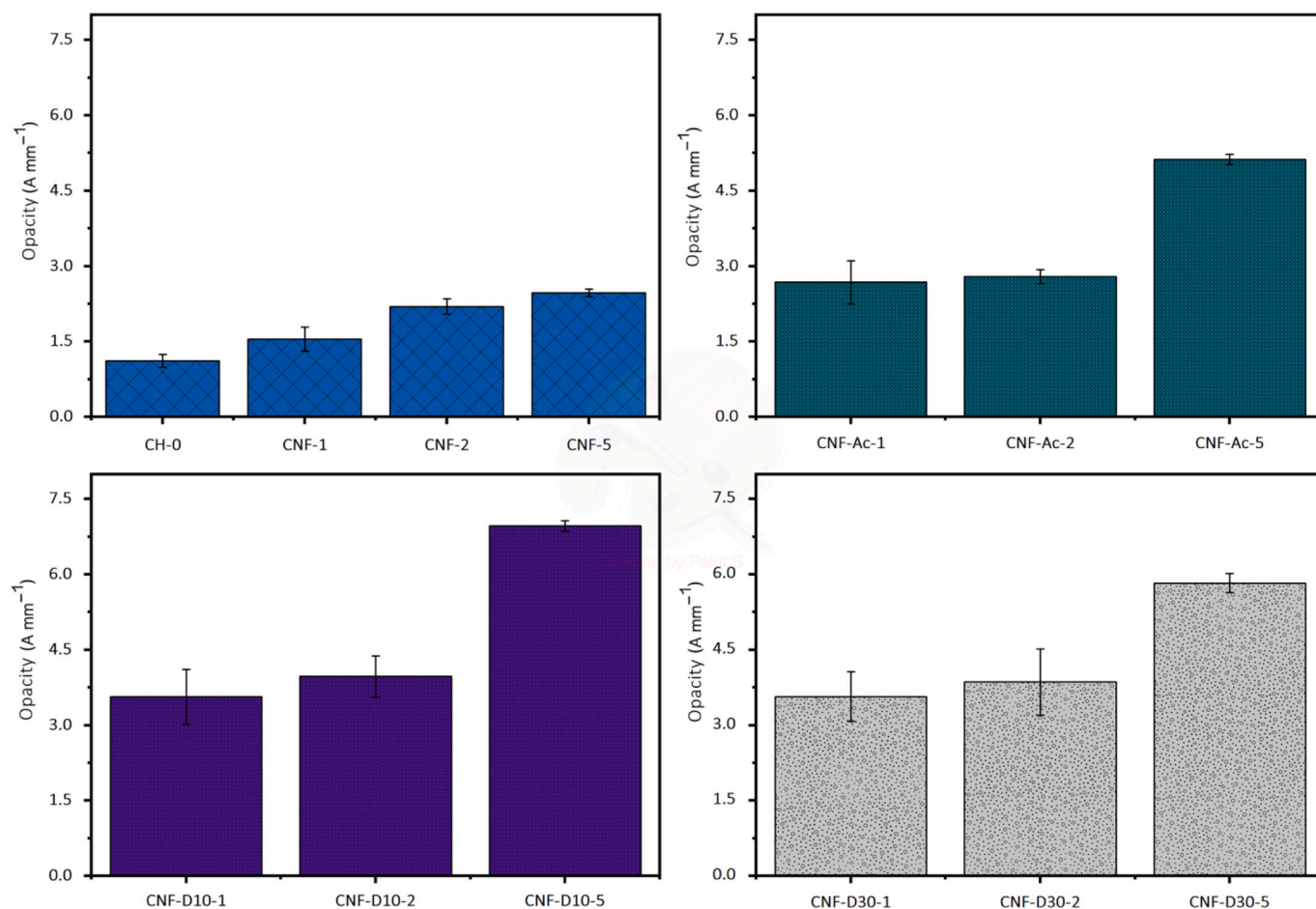
Fig. 7. Opacity analysis of the copolymerized cellulose nanofibers and copolymerized cellulose nanofibers/diatomite/chitosan composite films. Mean values ± standard deviation ($n = 3$).

reported Akyuz et al. (2017). This decrease in *Tr* can be attributed to the interaction between diatomite and chitosan, making it difficult for light to penetrate the nanocomposite films. Concerning the UV light, all nanocomposite films showed a decrease in *Tr* as <40% at the wavelength of ≈345 nm. However, the sample CNF-D30-5, which contains a higher percentage of diatomite and CNF, showed a value close to *Tr* as 0%, indicating a complete blockage of UV light. In general, all the films showed a lower transmittance value in the range of 250–750 nm compared to pure chitosan film. These results indicated that the addition of diatomite and CNF could improve the barrier properties of the chitosan-based films against UV light.

Besides film transparency, color is another crucial factor determining the application of films. The effect of different reinforcements on the nanocomposite film color was evaluated, and the results are given in Fig. 9. Full values are presented in Table S5. The incorporation of CNFs and CNF-D notably affected the color of the nanocomposite films, with a direct relationship between the reinforcement content and the color change (ΔE) being more notorious for samples with diatomite, having a distinct difference in +b* related with the yellowish color of diatomaceous earth.

3.6. Soil degradation and water solubility

Biodegradability is an essential parameter for food-packaging films. It is crucial to produce easily degradable and environmentally friendly films for coating or packaging purposes. The degradation results of the samples in the soil after 15 days are in Table S4. The soil degradation of CH-0 was found to be 30.7%. Soil biodegradability of CNF-1, CNF-2, and

CNF-5 composite films was recorded as 30.7%, 27.16%, and 23.3%, respectively. The degradation of CNF-reinforced chitosan films was reduced with the increase of CNF, as their incorporation resulted in a strong interaction between the matrix and filler (Deepa et al., 2016). Thus, the deterioration of the films becomes difficult due to the difficulty in breaking the strong bonds between matrix and reinforcement. For CNF-Ac-1, CNF-Ac-2, and CNF-Ac-5 films, soil degradation has been determined as 15.7%, 33.0%, and 35.1%, respectively. Compared to CH-0, it was observed that the biodegradability increased by increasing the concentration of polyacrylonitrile. CNF-D10-1. CNF-D10-2 and CNF-D10-5 soil solubility were 37.08, 24.61, and 31.3%, respectively, while CNF-D30-1. CNF-D30-2 and CNF-D30-5 it was 34.3, 25.8, and 11.1%, respectively. As can be seen from the increase of PD, there was an increase in the biodegradability, as the diatomite, being earth, goes back to the soil easily, thus helping the process of decomposition of the reinforced films.

Water solubility is crucial for the production of food packaging materials. For functional food packaging materials, maintaining its structural integrity is important when it comes to contact with water; otherwise, the applications will be restricted. Therefore, it is important to develop films insoluble in water. The water solubility of CH-0 and composite films is shown in Table S4. The water solubility of CH-0 was 30%. For CNF-1, CNF-2, and CNF-5, the water solubility was 28.3%, 26.3%, and 24.2%, respectively. It was observed that the amount of CNF proportionally decreased water solubility. This can be attributed to the formation of hydrogen bonding between the CNF and the chitosan film matrix. Cellulose nanofibers and chitosan share a large set of similar functional groups such as hydroxyl (OH) stretching vibration, alkane
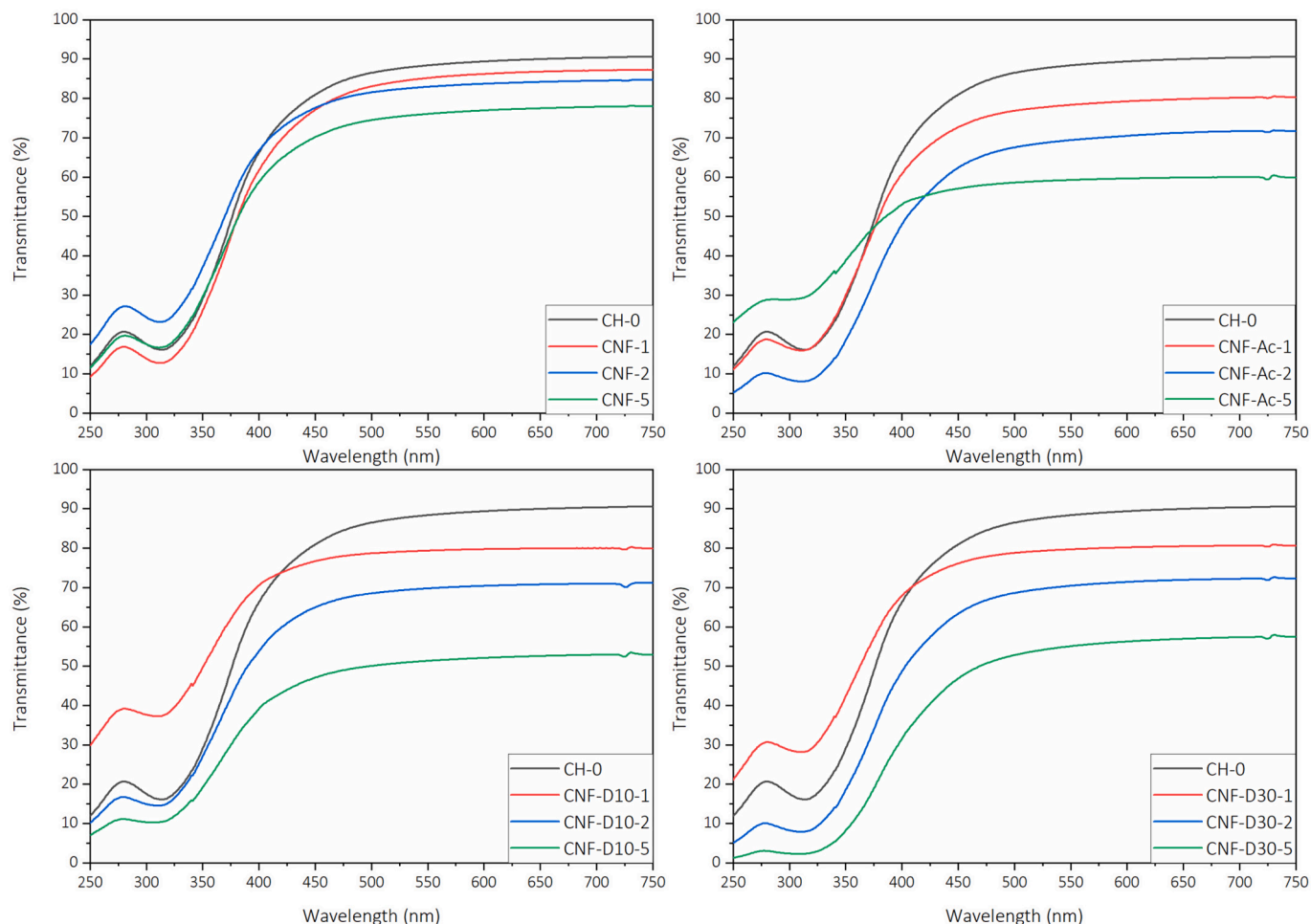
Fig. 8. UV–Vis spectra of the copolymerized cellulose nanofibers, and copolymerized cellulose nanofibers/diatomite/chitosan composite films from 245 to 750 nm.

C—H stretching vibration, and C—O stretching vibration. The IR bands at 3000 and 3400 cm^{-1} can be assigned as OH bands attributed to the hydroxyl and amino groups stretching vibration. In a similar study, the addition of CNF resulted in reduced water solubility of alginate-based films (Deepa et al., 2016). In CNF-Ac-1, CNF-Ac-2, and CNF-Ac-5, water solubility was 28.7, 26.6, and 23.5%, respectively. It was observed that water solubility decreased by increasing the proportion of CNF-Ac because of the crosslinking feature of polyacrylonitrile, which adds new physical properties to the film matrix, including reduced water solubility (Nam et al., 2001). Although water molecules tend to penetrate the polymer matrix and eliminate the force of interaction between polymer molecules, CNF-Ac made water-solubility of composite films difficult as the CNF has strongly copolymerized with polyacrylonitrile. In samples containing diatomite, CNF-D10-1, CNF-D10-2, and CNF-D10-5 had a water solubility of 30.3, 29.90, and 21.7%, respectively.

On the other hand, CNF-D30-1, CNF-D30-2, and CNF-D30-5 has solubility values as 29.9, 28.1, and 21%, respectively. It is observed that the solubility decreases as the diatomite increases. This can be due to the hydrophobic character of diatomite. It is known that the water solubility of diatomite is less than 1% by its nature (Parkinson & Gordon, 1999). The changes in elasticity of the composite films are also related to the increase in solid content as it affects the overall water molecules mobility in the matrix. Besides, a study has been found that the chitosan-diatomite film shows hydrophobic properties (Akyuz et al., 2017). It is predicted that the films produced, especially those with additives to diatomite, maybe a good food packaging material.

4. Conclusions

For the first time, the combined effect of copolymerized cellulose nanofibers and diatomite over the physiological and biological properties of chitosan films was investigated in the current study. Results revealed a successful enhancement in the mechanical properties, hydrophobicity, as studied by the water contact angle, their antioxidant activity, and the composite films' degradation properties. The increase of the diatomite share in the composites did not influence the antioxidant activity. The overall improvement of the selected properties can be ascribed to a successful bond formation between chitosan molecules, diatomite, and CNFs. On the other hand, the thermal stability did not reveal any notable change after incorporating diatomite and copolymerized CNFs. Moreover, the SEM images showed a partial homogenous distribution of diatomite and CNFs in the chitosan matrix. It was concluded that the incorporation of copolymerized CNFs and diatomite are suitable reinforcing candidates, which can be, utilized for increasing the mechanical and other listed properties of any composite film. Besides, based on the current results the produced composite combination can be tested for food packaging (coating for shelf-life extension assay) application. Extensive biological assays describing the toxicity analysis and antimicrobial potential are required to exploit the other potential applications.

CRediT authorship contribution statement

Muhammad Mujtaba: Conceptualization, Investigation, Writing – original draft, Validation, Methodology. **Rut Fernandez-Marín:**
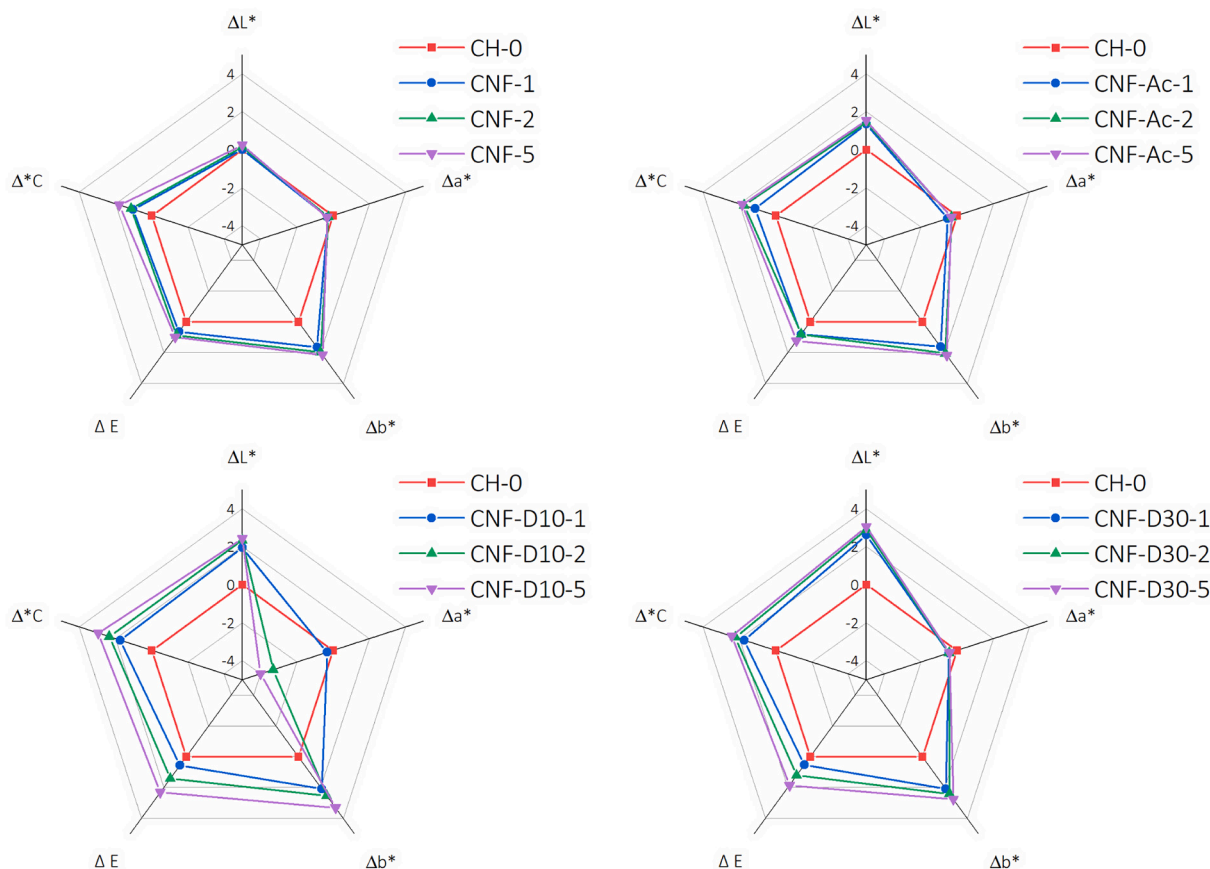
Fig. 9. Color changes of the reinforced films compared with the blank film (CH-0).

Investigation, Methodology, Writing – original draft, Writing – review & editing. **Eduardo Robles:** Writing – original draft, Methodology, Formal analysis, Visualization. **Jalel Labidi:** Supervision, Resources, Funding acquisition, Validation, Writing – review & editing. **Bahar Akyuz Yıl-maz:** Investigation, Writing – original draft. **Houwaida Nefzi:** Investigation, Writing – original draft.

Appendix A. Supplementary data

Supplementary data to this article can be found online at https://doi. org/10.1016/j.carbpol.2021.118424.

References

Ahyat, N. M., Mohamad, F., Ahmad, A., & Azmi, A. A. (2017). Chitin and chitosan extraction from portunus pelagicus. *Malays. J. Anal. Sci., 21,* 770–777.

Akyuz, L., Kaya, M., Koc, B., Mujtaba, M., Ilk, S., Labidi, J., … Yildiz, A. (2017). Diatomite as a novel composite ingredient for chitosan film with enhanced physicochemical properties. *International Journal of Biological Macromolecules, 105,* 1401–1411.

Andonegi, M., Las Heras, K., Santos-Vizcaíno, E., Igartua, M., Hernandez, R. M., de la Caba, K., & Guerrero, P. (2020). Structure-properties relationship of chitosan/collagen films with potential for biomedical applications. *Carbohydrate Polymers, 237,* Article 116159.

Anitha, T., Kumar, P. S., Kumar, K. S., Ramkumar, B., & Ramalingam, S. (2015). Adsorptive removal of Pb (II) ions from polluted water by newly synthesized chitosan–polyacrylonitrile blend: Equilibrium, kinetic, mechanism and thermodynamic approach. *Process Safety and Environmental Protection, 98,* 187–197.

ASTM, D. (1995). Standard test method for tensile properties of thin plastic sheeting. In *Annual books of ASTM standards: Designation* (pp. 882–895).

Bonilla, J., Poloni, T., Lourenço, R. V., & Sobral, P. J. (2018). Antioxidant potential of eugenol and ginger essential oils with gelatin/chitosan films. *Food Bioscience, 23,* 107–114.

Cardenas, G., & Miranda, S. P. (2004). FTIR and TGA studies of chitosan composite films. *Journal of the Chilean Chemical Society, 49*(4), 291–295.

Celebi, H., & Kurt, A. (2015). Effects of processing on the properties of chitosan/cellulose nanocrystal films. *Carbohydrate Polymers, 133,* 284–293.

Deepa, B., Abraham, E., Pothan, L. A., Cordeiro, N., Faria, M., & Thomas, S. (2016). Biodegradable nanocomposite films based on sodium alginate and cellulose nanofibrils. *Materials, 9*(1), 50.

Deng, Z., Jung, J., & Zhao, Y. (2017). Development, characterization, and validation of chitosan adsorbed cellulose nanofiber (CNF) films as water resistant and antibacterial food contact packaging. *LWT - Food Science and Technology, 83,* 132–140.

Dong, Y., Ruan, Y., Wang, H., Zhao, Y., & Bi, D. (2004). Studies on glass transition temperature of chitosan with four techniques. *Journal of Applied Polymer Science, 93* (4), 1553–1558.

Duan, B., Sun, P., Wang, X., & Yang, C. (2011). Preparation and properties of starch nanocrystals/carboxymethyl chitosan nanocomposite films. *Starch-Stärke, 63*(9), 528–535.

Earnest, C. M. (1988). *Compositional analysis by thermogravimetry.* ASTM International.

Fan, W., Sun, J., Chen, Y., Qiu, J., Zhang, Y., & Chi, Y. (2009). Effects of chitosan coating on quality and shelf life of silver carp during frozen storage. *Food Chemistry, 115*(1), 66–70.

Fernández-Marín, R., Labidi, J., Andrés, M.Á., & Fernandes, S. C. (2020). Using α-chitin nanocrystals to improve the final properties of poly (vinyl alcohol) films with Origanum vulgare essential oil. *Polymer Degradation and Stability, 179,* Article 109227.

Gürdağ, G., & Sarmad, S. (2013). Cellulose graft copolymers: Synthesis, properties, and applications. In S. Kalia, & M. W. Sabaa (Eds.), *Polysaccharide based graft copolymers* (pp. 15–57). Berlin, Heidelberg: Springer Berlin Heidelberg.

H.P.S., A. K., Saurabh, C. K., A.S., A., Nurul Fazita, M. R., Syakir, M. I., Davoudpour, Y., … Dungani, R. (2016). A review on chitosan-cellulose blends and nanocellulose reinforced chitosan biocomposites: Properties and their applications. *Carbohydrate Polymers, 150*, 216–226.

Hai, L. V., Zhai, L., Kim, H. C., Panicker, P. S., Pham, D. H., & Kim, J. (2020). Chitosan nanofiber and cellulose nanofiber blended composite applicable for active food packaging. *Nanomaterials, 10*(9).

Jahed, E., Khaledabad, M. A., Almasi, H., & Hasanzadeh, R. (2017). Physicochemical properties of Carum copticum essential oil loaded chitosan films containing organic nanoreinforcements. *Carbohydrate Polymers, 164*, 325–338.

Kalaoğlu, Ö.İ., Ünlü, C. H., & Atıcı, O. G. (2016). Synthesis, characterization and electrospinning of corn cob cellulose-graft-polyacrylonitrile and their clay nanocomposites. *Carbohydrate Polymers, 147*, 37–44.

Kaya, M., Khadem, S., Cakmak, Y. S., Mujtaba, M., Ilk, S., Akyuz, L., … Deligöz, E. (2018). Antioxidative and antimicrobial edible chitosan films blended with stem, leaf and seed extracts of Pistacia terebinthus for active food packaging. *RSC Advances, 8*(8), 3941–3950.

Khan, A., Khan, R. A., Salmieri, S., Le Tien, C., Riedl, B., Bouchard, J., … Lacroix, M. (2012). Mechanical and barrier properties of nanocrystalline cellulose reinforced chitosan based nanocomposite films. *Carbohydrate Polymers, 90*(4), 1601–1608.

Kim, J.-N., Lee, J., Go, T. W., Rajabi-Abhari, A., Mahato, M., Park, J. Y., … Oh, I.-K. (2020). Skin-attachable and biofriendly chitosan-diatom triboelectric nanogenerator. *Nano Energy, 75*, Article 104904.

Kim, J.-N., Lee, J., Lee, H., & Oh, I.-K. (2021). Stretchable and self-healable catechol-chitosan-diatom hydrogel for triboelectric generator and self-powered tremor sensor targeting at Parkinson disease. *Nano Energy, 82*, Article 105705.

Kim, S. S., & Lee, J. (2014). Antibacterial activity of polyacrylonitrile–chitosan electrospun nanofibers. *Carbohydrate Polymers, 102*, 231–237.

Kong, M., Chen, X. G., Xing, K., & Park, H. J. (2010). Antimicrobial properties of chitosan and mode of action: A state of the art review. *International Journal of Food Microbiology, 144*(1), 51–63.

Kurek, M., Ščetar, M., Voilley, A., Galić, K., & Debeaufort, F. (2012). Barrier properties of chitosan coated polyethylene. *Journal of Membrane Science, 403-404*, 162–168.

Labidi, A., Salaberria, A. M., Fernandes, S. C., Labidi, J., & Abderrabba, M. (2016). Adsorption of copper on chitin-based materials: Kinetic and thermodynamic studies. *Journal of the Taiwan Institute of Chemical Engineers, 65*, 140–148.

Li, Q., Zhou, J., & Zhang, L. (2009). Structure and properties of the nanocomposite films of chitosan reinforced with cellulose whiskers. *Journal of Polymer Science Part B: Polymer Physics, 47*(11), 1069–1077.

Liang, W., Yu, A., Wang, G., Zheng, F., Jia, J., & Xu, H. (2018). Chitosan-based nanoparticles of avermectin to control pine wood nematodes. *International Journal of Biological Macromolecules, 112*, 258–263.

Maiti, S., Sain, S., Ray, D., & Mitra, D. (2013). Biodegradation behaviour of PMMA/cellulose nanocomposites prepared by in-situ polymerization and ex-situ dispersion methods. *Polymer Degradation and Stability, 98*(2), 635–642.

Mujtaba, M., Koc, B., Salaberria, A. M., Ilk, S., Cansaran-Duman, D., Akyuz, L., … Boufi, S. (2019). Production of novel chia-mucilage nanocomposite films with starch nanocrystals; an inclusive biological and physicochemical perspective. *International Journal of Biological Macromolecules, 133*, 663–673.

Mujtaba, M., Morsi, R. E., Kerch, G., Elsabee, M. Z., Kaya, M., Labidi, J., & Khawar, K. M. (2019). Current advancements in chitosan-based film production for food technology; a review. *International Journal of Biological Macromolecules, 121*, 889–904.

Mujtaba, M., Salaberria, A. M., Andres, M. A., Kaya, M., Gunyakti, A., & Labidi, J. (2017). Utilization of flax (Linum usitatissimum) cellulose nanocrystals as reinforcing material for chitosan films. *International Journal of Biological Macromolecules, 104*, 944–952.

Mujtaba, M., Sargin, I., & Kaya, M. (2018). Determination of bovine serum albumin adsorption capacity of newly obtained cellulose extracted from Glycyrrhiza glabra (Licorice). *Advances in Polymer Technology, 37*(2), 606–611.

Nam, C. W., Kim, Y. H., & Ko, S. W. (2001). Blend fibers of polyacrylonitrile and water-soluble chitosan derivative prepared from sodium thiocyanate solution. *Journal of Applied Polymer Science, 82*(7), 1620–1629.

Nefzi, H., Abderrabbaa, M., Ayadia, S., & Labidic, J. (2019). Cellulose modified diatomite for toluene removal from aqueous solution. *Desalination and Water Treatment, 150*, 228–236.

Nefzi, H., Abderrabba, M., Ayadi, S., & Labidi, J. (2018). Formation of palygorskite clay from treated diatomite and its application for the removal of heavy metals from aqueous solution. *Water, 10*(9), 1257.

Noorbakhsh-Soltani, S. M., Zerafat, M. M., & Sabbaghi, S. (2018). A comparative study of gelatin and starch-based nano-composite films modified by nano-cellulose and chitosan for food packaging applications. *Carbohydrate Polymers, 189*, 48–55.

Parkinson, J., & Gordon, R. (1999). Beyond micromachining: The potential of diatoms. *Trends in Biotechnology, 17*(5), 190–196.

Pennells, J., Godwin, I. D., Amiralian, N., & Martin, D. J. (2020). Trends in the production of cellulose nanofibers from non-wood sources. *Cellulose*, 1–19.

Pereda, M., Ponce, A., Marcovich, N., Ruseckaite, R., & Martucci, J. (2011). Chitosan-gelatin composites and bi-layer films with potential antimicrobial activity. *Food Hydrocolloids, 25*(5), 1372–1381.

Priyadarshi, R., Kumar, B., Deeba, F., Kulshreshtha, A., & Negi, Y. S. (2018). Chitosan films incorporated with Apricot (Prunus armeniaca) kernel essential oil as active food packaging material. *Food Hydrocolloids, 85*, 158–166.

Rambabu, K., Bharath, G., Banat, F., Show, P. L., & Cocoletzi, H. H. (2019). Mango leaf extract incorporated chitosan antioxidant film for active food packaging. *International Journal of Biological Macromolecules, 126*, 1234–1243.

Resende, N., Gonçalves, G., Reis, K., Tonoli, G., & Boas, E. (2018). Chitosan/cellulose nanofibril nanocomposite and its effect on quality of coated strawberries. *Journal of Food Quality, 2018*.

Robles, E., Fernández-Rodríguez, J., Barbosa, A. M., Gordobil, O., Carreño, N. L. V., & Labidi, J. (2018). Production of cellulose nanoparticles from blue agave waste treated with environmentally friendly processes. *Carbohydrate Polymers, 183*, 294–302.

Romainor, A. N. B., Chin, S. F., Pang, S. C., & Bilung, L. M. (2014). Preparation and characterization of chitosan nanoparticles-doped cellulose films with antimicrobial property. *Journal of Nanomaterials, 2014*.

Roy, D., Guthrie, J. T., & Perrier, S. (2005). Graft polymerization: Grafting poly (styrene) from cellulose via reversible addition–fragmentation chain transfer (RAFT) polymerization. *Macromolecules, 38*(25), 10363–10372.

Sakurai, K., Maegawa, T., & Takahashi, T. (2000). Glass transition temperature of chitosan and miscibility of chitosan/poly (N-vinyl pyrrolidone) blends. *Polymer, 41*(19), 7051–7056.

Schreiber, S. B., Bozell, J. J., Hayes, D. G., & Zivanovic, S. (2013). Introduction of primary antioxidant activity to chitosan for application as a multifunctional food packaging material. *Food Hydrocolloids, 33*(2), 207–214.

Sharif, R., Mujtaba, M., Ur Rahman, M., Shalmani, A., Ahmad, H., Anwar, T., … Wang, X. (2018). The multifunctional role of chitosan in horticultural crops; a review. *Molecules, 23*(4), 872.

Soni, B., Schilling, M. W., & Mahmoud, B. (2016). Transparent bionanocomposite films based on chitosan and TEMPO-oxidized cellulose nanofibers with enhanced mechanical and barrier properties. *Carbohydrate Polymers, 151*, 779–789.

Tamburaci, S., & Tihminlioglu, F. (2017). Diatomite reinforced chitosan composite membrane as potential scaffold for guided bone regeneration. *Materials Science and Engineering, C, 80*, 222–231.

Tirkistani, F. A. (1998). Thermal analysis of some chitosan Schiff bases. *Polymer Degradation and Stability, 60*(1), 67–70.

Tripathi, S., Mehrotra, G., & Dutta, P. (2009). Physicochemical and bioactivity of cross-linked chitosan–PVA film for food packaging applications. *International Journal of Biological Macromolecules, 45*(4), 372–376.

Wang, H., Qian, J., & Ding, F. (2018). Emerging chitosan-based films for food packaging applications. *Journal of Agricultural and Food Chemistry, 66*(2), 395–413.

Wu, C., Sun, J., Zheng, P., Kang, X., Chen, M., Li, Y., … Pang, J. (2019). Preparation of an intelligent film based on chitosan/oxidized chitin nanocrystals incorporating black rice bran anthocyanins for seafood spoilage monitoring. *Carbohydrate Polymers, 222*, Article 115006.

Wu, Z., Huang, X., Li, Y.-C., Xiao, H., & Wang, X. (2018). Novel chitosan films with laponite immobilized Ag nanoparticles for active food packaging. *Carbohydrate Polymers, 199*, 210–218.

Xu, C., Wang, G., Xing, C., Matuana, L. M., & Zhou, H. (2015). Effect of graphene oxide treatment on the properties of cellulose nanofibril films made of banana petiole fibers. *BioResources, 10*(2), 2809–2822.

Xu, J., Xia, R., Yuan, T., & Sun, R. (2019). Use of xylooligosaccharides (XOS) in hemicelluloses/chitosan-based films reinforced by cellulose nanofiber: Effect on physicochemical properties. *Food Chemistry, 298*, Article 125041.

Xu, Y. X., Kim, K. M., Hanna, M. A., & Nag, D. (2005). Chitosan–starch composite film: Preparation and characterization. *Industrial Crops and Products, 21*(2), 185–192.

Zhang, C., Yang, X., Li, Y., Qiao, C., Wang, S., Wang, X., … Li, T. (2020). Enhancement of a zwitterionic chitosan derivative on mechanical properties and antibacterial activity of carboxymethyl cellulose-based films. *International Journal of Biological Macromolecules, 159*, 1197–1205.

Zhao, K., Wang, W., Teng, A., Zhang, K., Ma, Y., Duan, S., … Guo, Y. (2020). Using cellulose nanofibers to reinforce polysaccharide films: Blending vs layer-by-layer casting. *Carbohydrate Polymers, 227*, Article 115264.

Zhao, Y., Huerta, R. R., & Saldaña, M. D. (2019). Use of subcritical water technology to develop cassava starch/chitosan/gallic acid bioactive films reinforced with cellulose nanofibers from canola straw. *The Journal of Supercritical Fluids, 148*, 55–65.